Fast analysis of gap waveguides using the characteristic basis function method and the parallel-plate Green's function

Fast Analysis of Gap Waveguides Using the Characteristic Basis Function Method and the Parallel-Plate Green's Function

R. Maaskant* P. Takook† P.-S. Kildal‡

Abstract — **The Characteristic Basis Function Method is employed in conjunction with the parallel-plate dyadic Green's function method to obtain the impedance characteristics of electrically large gap-waveguide structures. Numerical results are shown for the groove gap waveguide demonstrating reduced execution times relative to the HFSS software, while the solution accuracy is barely compromised.**

1 INTRODUCTION

To anticipate to future trends in high-frequency electronics, a novel low-loss low-cost waveguide and transmission-line technology has been proposed – referred to as the gap waveguide technology [1]. The basic structure consists of a pair of perfect electric conducting (PEC) top and bottom ground planes in conjunction with a bed of nails for realizing a perfect magnetic conductor (PMC) boundary condition. Fig. 1 illustrates an example of a groove

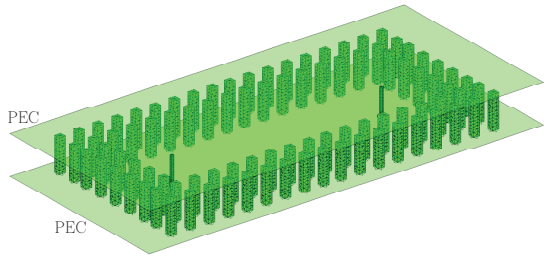

Figure 1: Coaxial-probe excited groove gap waveguide.

gap waveguide, where two coaxial probes are used to excite the waveguide fields. The groove is bordered by only a few rows of pins to prevent the fields from leaking out (sideways) when operating in the stop band. The pins are electrically interconnected to the bottom PEC plate, while no electrical contact between the pins and the upper PEC plate is required. The so-formed capacitive gap in the "gap waveguide" is not only needed to realize the PMC, but represents a mechanical advantage as well.

To allow for a fast analysis and optimization of gap waveguides, it is required to develop tailored computational electromagnetic methods that are numerically efficient. In this paper, we propose to employ the Characteristic Basis Function Method (CBFM, [2]) in conjunction with the parallel-plate Green's function [3]. This methodology enhances the computational efficiency of conventional method of moment (MoM) codes significantly. Furthermore, the CBFM is memory efficient and allows us to solve problems that are typically 1–3 orders larger in size.

2 PARALLEL PLATE DYADIC GREEN'S FUNCTION

Consider Fig. 2, where the EM field of a dipole point source inside a parallel-plate region is computed with the help of the image principle. Depending upon whether the dipole has an x-, y-, or z-orientation, the field for each polarization is regarded as being radiated by two superimposed 1D-line arrays of dipole point sources with the original and possibly mirrored polarization, respectively. Each line array has an inter-dipole spacing of twice the plate distance. In Dyadic form, the spatial parallel-plate Green's function $\mathbf{G}$ is expressed as $\mathbf{G}(\boldsymbol{r},\boldsymbol{r}') = G^N_{xx}\hat{\boldsymbol{x}}\hat{\boldsymbol{x}}^T + G^N_{yy}\hat{\boldsymbol{y}}\hat{\boldsymbol{y}}^T + G^N_{zz}\hat{\boldsymbol{z}}\hat{\boldsymbol{z}}^T$, where

$$
\begin{aligned}
G^N_{xx} &= \sum_{n=-N}^{N} \frac{e^{-jk_0\sqrt{\rho^2+(z-z'+2dn)^2}}}{4\pi\sqrt{\rho^2+(z-z'+2dn)^2}} \\
&\quad - \sum_{n=-N}^{N} \frac{e^{-jk_0\sqrt{\rho^2+(z+z'+2d(n-1))^2}}}{4\pi\sqrt{\rho^2+(z+z'+2d(n-1))^2}} \\
G^N_{yy} &= G^N_{xx} \\
G^N_{zz} &= \sum_{n=-N}^{N} \frac{e^{-jk_0\sqrt{\rho^2+(z-z'+2dn)^2}}}{4\pi\sqrt{\rho^2+(z-z'+2dn)^2}} \\
&\quad + \sum_{n=-N}^{N} \frac{e^{-jk_0\sqrt{\rho^2+(z+z'+2d(n-1))^2}}}{4\pi\sqrt{\rho^2+(z+z'+2d(n-1))^2}}
\end{aligned}
\tag{1}
$$

*Chalmers University of Technology, Dept. of Signals and Systems, 412 96, Gothenburg , Sweden, e-mail: rob.maaskant@chalmers.se

†Chalmers University of Technology, Dept. of Signals and Systems, 412 96, Gothenburg , Sweden, e-mail: takook@student.chalmers.se

‡Chalmers University of Technology, Dept. of Signals and Systems, 412 96, Gothenburg , Sweden, e-mail: per-simon.kildal@chalmers.se

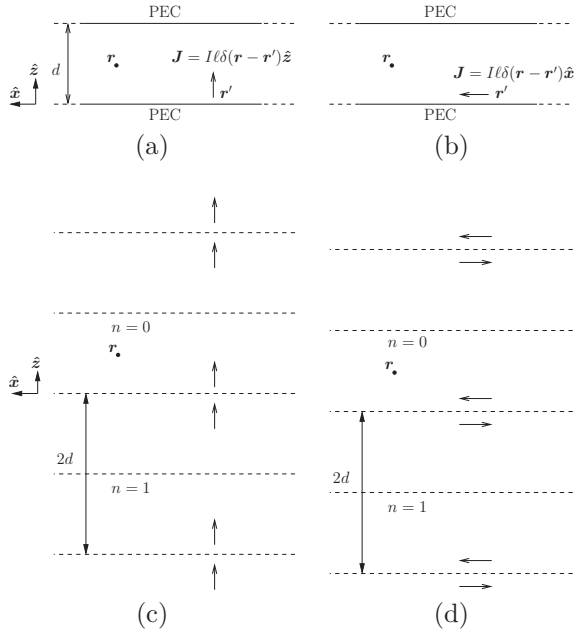

Figure 2: (a) z-polarized and (b) x-polarized electric Hertzian dipole currents in between two infinitely large parallel PEC plates separated by a distance d; (c) and (d), the repeated application of the image principle for both dipole polarizations, respectively.

for $N \to \infty$, and where we have defined that $\rho^2 = (x-x')^2 + (y-y')^2$. It is well-known that each summation in Eq. (1) is performed over a slowly convergent series. However, the field of a line array can be computed rapidly using the Shanks-accelerated spatial Green's function method. Other methods, such as the Ewald summation method, or the spectral-domain summation method, were found to be less efficient for our type of problems [3]. For instance, the Ewald summation method requires very few terms in the near-field region of the source, but the computation time of a single term is orders larger than that of a spatial Green's function term. Furthermore, if only a few digits accuracy is required, which is often sufficiently good, only a few terms are needed. In fact, we found that for our type of problems, the overall series evaluation time is shortest for the Shanks-accelerated spatial Green's function method. Finally, we point out that the Shanks transformation is easy to implement. For example, when considering the new series G_{xx}^N, for $N = 1, 2, \ldots$, the extrapolated value for $N \to \infty$ is

$$G_{xx}^{\infty} \approx \frac{G_{xx}^{N+1} G_{xx}^{N-1} - \left(G_{xx}^{N}\right)^2}{G_{xx}^{N+1} - 2G_{xx}^{N} + G_{xx}^{N-1}} \qquad (2)$$

where N is taken sufficiently large. We concluded that the double Shanks tranformation on the orignal spatial Green's function series represents the best trade off between the solution accuracy and the total series evaluation time [3].

3 CHARACTERISTIC BASIS FUNCTION METHOD

To minimize the total number of basis functions, entire-domain basis functions are employed for the electric surface currents on the conductors inside the gap waveguide; in this specific case on the pins and coaxial probes only. Each of these so-called Characteristic Basis Functions (CBFs) is expanded in terms of a fixed combination of lower-level basis functions, which are herein chosen to be the Rao-Wilton-Glisson (RWG) basis functions. The CBFs are generated for a small part of the structure only, namely by solving for the current in the corresponding subdomain. As an example, consider Fig. 3, where the CBFs are generated for one of the pins. Here, each pin consists of 382 RWGs. A

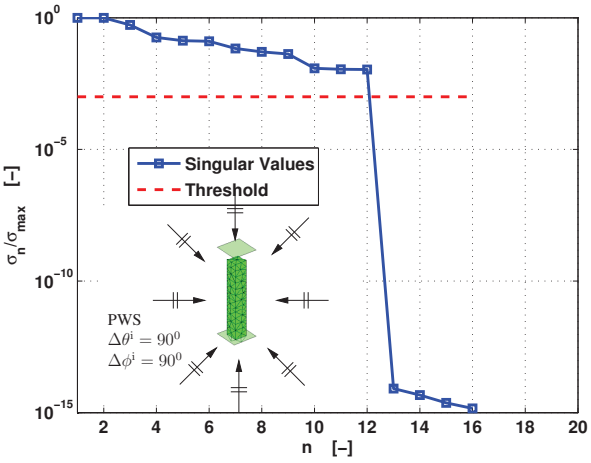

Figure 3: Generation of CBFs on a pin using a plane wave spectrum (PWS). The singular value spectrum is shown where a threshold is used to limit the maximum number of employed CBFs.

plane wave spectrum is incident on the pin with $\Delta\theta^{\mathrm{i}} = \Delta\phi^{\mathrm{i}} = 90^0$ (and two polarizations). This generates 16 currents on the pin. The currents are stored as RWG expansion coefficients vectors and make up the columns of the matrix $\mathbf{J} = \mathbf{UDV}^H$, where the right-hand side is the SVD of $\mathbf{J}$. The magnitude of the normalized singular values in $\mathbf{D}$ are plotted in Fig. 3. With an appropriate thresholding procedure on the singular values, only the first 12 column vectors of the left-singular matrix $\mathbf{U}$ are retained and subsequently used as CBFs. The

reduction in the number of unknowns per pin is therefore 382/12=31.8 (@ 12 GHz).

Since the set of CBFs is identical for each pin, we use symmetry to generate a set for all the pins through translation [4]. The same procedure is followed for the coaxial probes. More details on the generation of CBFs can be found in [2], where also electrically interconnected subdomains are considered.

After generating the CBFs for all M subdomains, i.e., $\mathbf{J}_m$, for $m = 1, 2, \ldots, M$, one can construct the reduced moment matrix equation $\mathbf{Z}^{\text{red}}\mathbf{I}^{\text{red}} = \mathbf{V}^{\text{red}}$, where

$$\mathbf{Z}^{\text{red}} = \begin{bmatrix} (\mathbf{J}_1)^T \mathbf{Z}_{11}\mathbf{J}_1 & \cdots & (\mathbf{J}_1)^T \mathbf{Z}_{1M}\mathbf{J}_M \\ \vdots & \ddots & \vdots \\ (\mathbf{J}_M)^T \mathbf{Z}_{M1}\mathbf{J}_1 & \cdots & (\mathbf{J}_M)^T \mathbf{Z}_{MM}\mathbf{J}_M \end{bmatrix} \tag{3}$$

and

$$\mathbf{V}^{\text{red}} = \left[(\mathbf{J}_1)^T \mathbf{V}_1, \cdots, (\mathbf{J}_M)^T \mathbf{V}_M \right]^T \tag{4}$$

and where the elements of the matrix block $\mathbf{Z}_{mn}$ are the reaction integrals between the RWG basis functions on the nth source and mth observation subdomain, respectively. Likewise, $\mathbf{V}_m$ is the original RWG voltage excitation vector for the mth subdomain, where the incident electric field is generated by the impressed magnetic frill currents that are supported by the coaxial apertures. This CBFM procedure leads to a reduced MoM matrix equation which can be solved in-core using standard Gaussian elimination techniques.

One observes that the CBFM can be regarded as an enhancement technique for conventional MoM approaches, since the original MoM-matrix blocks and excitation vectors are reduced with the help of the above-described CBFs. Although the methodology is very general and independent of the Green's function, in this work the MoM is used to discretize an Electric Field Integral Equation (EFIE) for the electric current inside a parallel-plate waveguide region using Galerkins method and RWG basis and test functions.

Finally, the CBFM is memory efficient and allows us to solve problems that are many wavelengths in size, even though the structure exhibits very fine geometrical features requiring detailed discretizations (multi-scale features).

4 Numerical Results

In this section the numerical results on the groove gap waveguide are presented, whose geometrical dimensions are as described in Table 1. Additionally,

Table 1: Geometrical dimensions of the Groove gap waveguide in [mm].

W_{pin}	H_{pin}	L_1	L_2	L_3	L_4
1	6.25	15.8	43.7	5.4	2

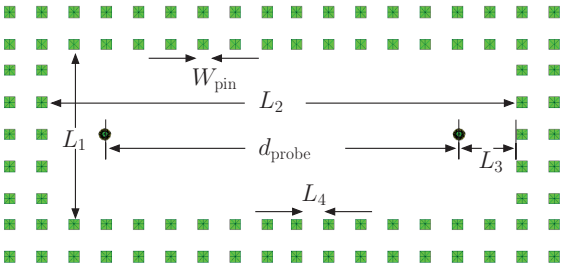

the radius and length of the coaxial probes are 0.25 and 5 mm, respectively. The parallel-plate distance $d = 7.25$ mm.

The CBFM computations have been carried out on a 64 bit (x86-64) Linux – openSUSE (v.11.4) server equipped with 2 Intel Xeon E5640 CPUs operating at 2.67 GHz (each CPU has 4 cores/8 threads), with access to 144 GB RAM memory and 2 TB harddisk space. The HFSS simulations were performed on a 64 bit Windows XP server equipped with 2 Intel Xeon 5130 CPUs operating at 2 GHz (each CPU has 2 cores/2 threads), 8 GB RAM, and 300 GB harddisk space.

Firstly, to verify the accuracy of CBFM, the 100-Ohm S-parameters for the gap waveguide structure (*cf.* Table 1) have been computed, both by our CBFM-enhanced MoM procedure and the HFSS software. In HFSS, the adaptive meshing terminates if the relative field error is less than 1%. The computed S-parameters for CBFM and HFSS are shown in Fig. 4 and are in good agreement. The solve times for this relatively small problem is 1 min. 41 sec. and 1 min. 24 sec. for CBFM and HFSS, respectively. The simulation times are comparable due to the relatively large overhead needed by the CBFM to determine the CBFs. The CBFM employed 37088 RWGs (1112 CBFs), while HFSS employed 42158 tetrahedra. Owing to the array structure, the meshing time is only 5 sec. for the CBFM, while it takes 3 min. 57 sec. for HFSS.

By changing L_2 one can examine the total solve time as a function of the problem size. The results are shown in Fig. 5, where the scaling of the solve time for CBFM outforms that of HFSS by about a factor of three. Also, for equal simulation times, the problem size for CBFM can be about twice larger than for the HFSS software. The HFSS software

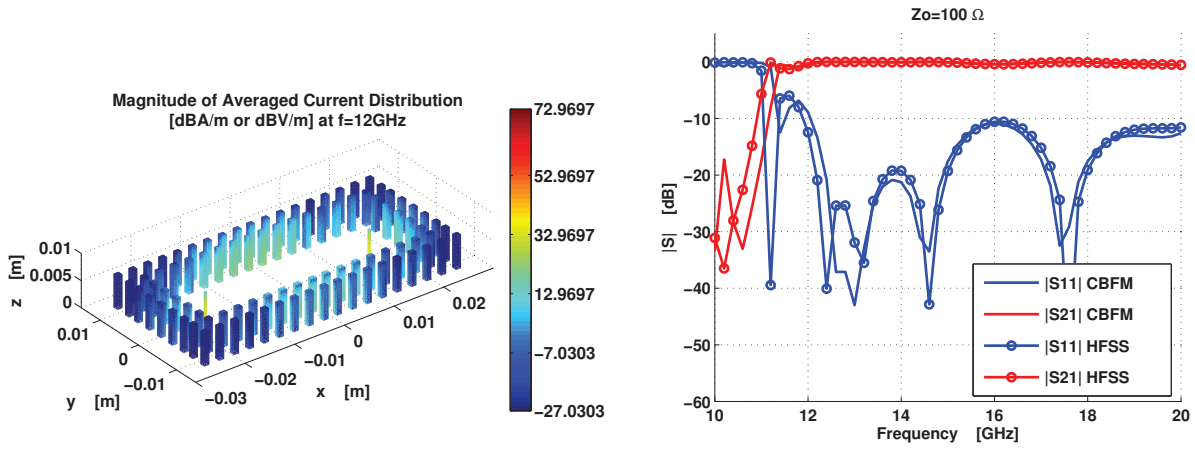

(a) (b)

Figure 4: (left) the magnitude of the computed electric current and S-parameters of a groove gap-waveguide when excited by a pair of coaxial probes; (right) the numerical results are computed by the CBFM employing the parallel-plate Greens function. The numerically computed results are validated through the HFSS software.

could not handle problems for $d_{\text{probe}} > 1.3$ m, due to memory constraints for that server. The non-gradual increase in simulation time is caused by the adaptive meshing of HFSS.

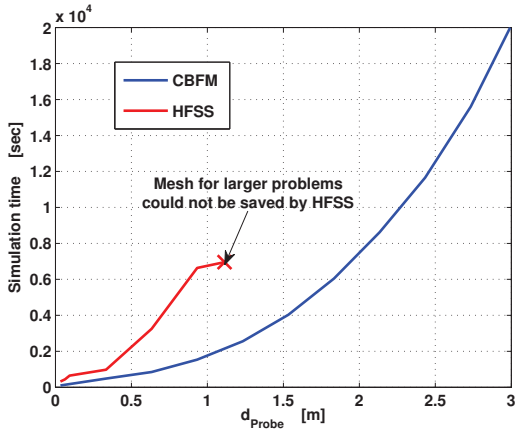

Figure 5: Scaling of the method: the total solve time as a function of problem size (d_{probe}).

5 Conclusions

The CBFM has been supplemented with the parallel-plate Green's function to enable the fast analysis of gap waveguide structures. By comparing the computed S-parameters obtained from CBFM and the HFSS software, it has been concluded that the solution accuracy for the CBFM is hardly compromised, while it is at least a factor three faster than the HFSS software.

Acknowledgments

This work is part of the research programme Rubicon, which is partly financed by the Netherlands Organization for Scientific Research (NWO).

References

[1] P.-S. Kildal, E. Alfonso, A. Valero-Nogueira, and E. Rajo-Iglesias, "Local metamaterial-based waveguides in gaps between parallel metal plates," *IEEE Antennas Wireless Propag. Lett.*, vol. 8, no. 1, pp. 84–87, 2009.

[2] R. Maaskant, R. Mittra, and A. G. Tijhuis, "Application of trapezoidal-shaped characteristic basis functions to arrays of electrically interconnected antenna elements," in *Proc. Int. Conf. on Electromagn. in Adv. Applicat. (ICEAA)*, Torino, Sep. 2007, pp. 567–571.

[3] P. Takook, R. Maaskant, and P.-S. Kildal, "Comparison of parallel-plate greens function acceleration techniques," in *Proc. European Conference on Antennas and Propag. (EuCAP)*, Prague, Czech Republic, Mar. 2012, pp. 1–5.

[4] R. Maaskant, R. Mittra, and A. G. Tijhuis, "Fast solution of multi-scale antenna problems for the square kilomtre array (SKA) radio telescope using the characteristic basis function method (CBFM)," Applied Computational Electromagnetics Society (ACES) Journal, vol. 24, no. 2, pp. 174–188, Apr. 2009.